Journal of Applied Fluid Mechanics, Vol. 17, No. 10, pp. 2141-2153, 2024.
Available online at www.jafmonline.net, ISSN 1735-3572, EISSN 1735-3645.
https://doi.org/10.47176/jafm.17.10.2548

Simulation of Very Low Frequency Pulsed Fluidized Bed

N. Abedi[1] and M. Nasr Esfahany[2†]

[1] *Chemical Engineering Group, Pardis College, Isfahan University of Technology, Isfahan 8415683111, Iran*
[2] *Department of Chemical Engineering, Isfahan University of Technology, Isfahan 8415683111, Iran*

†*Corresponding Author Email: mnasr@cc.iut.ac.ir*

ABSTRACT

Achieving high fluidization quality and bed stability is a paramount challenge in pulsed fluidized beds. 2D hydrodynamics models were studied using the Eulerian-Eulerian method with KTGF. This study investigates the impact of rectangular pulsation superimposed on steady airflow, while maintaining a constant temporal average gas velocity, on fluidization quality. Numerical results indicated that superimposing pulsations on steady airflow and increasing the steady airflow velocity to three times the minimum fluidization velocity resulted in a decrease in the bed expansion ratio. This decrease was most notable particularly at a pulsation frequency of 0.05Hz, with a reducing of approximately by about 21%. By decreasing the velocity ratio from 9.52 to 6.52, the pressure drop increased by 27% and 4.5% at 0.05 Hz and 10 Hz, respectively. Additionally, the fluidization index increased by 32% and 2% under these conditions. The optimal range of pulsed airflow velocity fell between 2.76 and 1.17 times the steady airflow velocity and was most effective at 0.05 – 0.1 Hz.

Article History

Received January 12, 2024
Revised April 5, 2024
Accepted May 3, 2024
Available online July 31, 2024

Keywords:

Combined airflow
CFD simulation
Fluidization quality
Pulsed fluidized bed
Pulse frequency

1. INTRODUCTION

Fluidized beds are extensively used in chemical, biochemical, and pharmaceutical industries because of their capability to maintain a uniform temperature and concentration within the bed (Kunii & Levenspiel, 1991; Taghipour et al., 2005; Laverman et al., 2008). Big bubble formation and bed instability are the main challenges encountered by particles with diameters ranging from 70 to 500 μm in fluidized beds (Huang & Levy, 2004; Dong et al., 2016). These issues arise due to the non-uniform distribution of particles, especially at high gas velocities. These challenges may result in poor heat and mass transfer during fluidization. The interaction between the collapse and transport of particles in the bed is referred to as bed stability. Various methods such as utilizing magnetic fields (Liu et al., 1991), electric fields (Van Willigen et al., 2005), acoustic excitation (Zhu et al., 2004), vibration (Feng et al., 2022), and pulsed flow (Oliveira et al., 2020) have been suggested to enhance the hydrodynamic performance of fluidized beds.

Pulsed flow is an operation in which the fluid velocity changes intermittently. It has the potential to overcome difficulties related to bed hydrodynamics, such as the formation of large bubbles, channeling, and gas bypassing (Zhang & Koksal, 2006; Dong et al., 2017; Mostafaei et al., 2020). Additionally, it can enhance bed stability (Li et al. 2020a) and gas-solid mixing (Shah et al., 2016). Fluidization quality is usually evaluated using the fluidization index and bed expansion ratio. The fluidization index is defined as the ratio of the maximum bed pressure drop to the hydrostatic pressure produced by the weight of bed materials (Nitz, 2007). The ratio of the maximum fluidization bed height to the static bed height is defined as the bed expansion ratio (Sau et al., 2010).

Numerous articles have recently been published on the hydrodynamics of pulsed fluidized beds. Massimilla (1966) experimentally investigated the different regimes of pulsed fluidization at various pulse frequencies. They observed that increasing the frequency changed the behavior of the bed from intermittent fluidization to full fluidization, thereby enhancing the bed operation. Wong and Baird (1971) studied the hydrodynamic behavior of pulsed fluidized beds at different frequencies ranging from 1 Hz to 10 Hz using a rectangular pulsation pattern. They observed that the shape of the bubbles fluctuated with the applied pulsation. Also, the uniform solid volume fraction was achieved at the highest pulse frequency (10 Hz) compared to steady flow.

Jia et al. (2015) investigated the fluidization of biomass particles with diameters ranging from 1.7 to 3.5 mm and high moisture content at frequencies ranging from 0.33 Hz to 6.67 Hz using a rectangular pulsation pattern. The regular bubble patterns were achieved at a pulse

NOMENCLATURE

A	cross sectional area of the bed	W	weight of particles
c	fluctuating solid velocity component	α	volume fraction
C_D	drag coefficient	γ_p	collision dissipation of energy
d_p	particle diameter	Θ	granular temperature
e_{pp}	restitution coefficient	λ	bulk viscosity
g	gravity acceleration	μ	shear viscosity
$g_{0,pp}$	radial distribution function	$\mu_{p,col}$	collisional part of the shear viscosity
H_{max}	maximum bed height	$\mu_{p,kin}$	kinetic viscosity
H_{static}	static bed height	$\mu_{p,fr}$	frictional viscosity
I	stress tensor	$k_{\Theta p}$	diffusion coefficient for granular energy
I_{2D}	second invariant of the deviatory stress tensor	φ_{qp}	generation energy
K_{pq}	gas-solid momentum exchange coefficient	i	general index
p	pressure	p	solid phase
ΔP	bed pressure drop	q	gas phase
R	interaction force between phases	max	maximum
Re	Reynolds number	ρ	density
u	velocity	τ	Reynolds stress tensor
FI	fluidization index	ϕ	internal friction angle

frequency of 6.67 Hz, which proved to be suitable. Wang and Rhodes (2005) also noted an enhancement in the mixing rate of particles with a diameter of 191 μm under a 5 Hz pulse frequency. The minimum fluidization velocity decreased, and the quality of fluidization improved with an increase in pulse frequency (Ireland et al., 2016). About a 75% reduction in the minimum fluidization velocity was achieved under pulsed flow by increasing the frequency up to 10 Hz compared to steady flow (Li et al., 2021). Köksal and Vural (1998) investigated the effect of pulsation on bubble size in a pulsed fluidized bed using turnip seeds. They observed a 40% reduction in bubble size at 4-6 Hz. Dong et al. (2021), Liu et al. (2016), and Li et al. (2010) found that as the frequency increased in a pulsed fluidized bed, the bubble size decreased, and the fluidization quality improved. Bizhaem and Tabriz (2013) experimentally investigated the hydrodynamics of a pulsed fluidized bed with an 11 cm diameter using three different particles of varying sizes. They used pulsed flow with a rectangular pattern at pulse frequencies ranging from 1 Hz to 10 Hz. Results showed that using pulsed flow and increasing the frequency up to 10 Hz decreased the minimum fluidization velocity, the bed surface oscillation, and the bed expansion ratio.

Jia et al. (2019) experimentally studied three different biomasses under various pulsation and gas velocities. By increasing the gas velocity, the contact between the gas and particles was improved. The authors observed that as the pulsed frequency increased, the intensity of pulsation decreased, resulting in undesirable flow behaviors such as channeling and defluidization. Results showed that an increase in the duty cycle leads to suitable fluidization behavior by increasing gas flow throughout the bed.

Computational Fluid Dynamics (CFD) simulation has been widely used as a powerful tool to study fluidized beds, in addition to experimental studies. Several studies have shown good agreement with experimental findings by using Eulerian-Eulerian modeling with the kinetic theory of granular flow (KTGF) in pulsed fluidized beds (Bizhaem & Tabriz, 2017; Nardo et al., 2018; Gao et al., 2020).

Li et al. (2020b) investigated particle mixing, heat transfer characteristics, and particle motion under various pulsed frequencies using numerical methods. Enhancing the mixing of gas-solid and achieving uniform contact was found to be possible by using pulsed flow in the fluidized bed. Li et al. (2021) conducted a numerical study on the flow characteristics in the pulsed fluidized bed. They observed that using pulsation leads to an increase in the velocity of particles. At different frequencies, the timing of bubble generation varies, and the most notable impact of pulsation on the flow characteristics was observed at 2.5 Hz.

Based on the reports published so far, high fluidization quality was achieved by utilizing only pulsed flow at high frequencies. High pulse frequency is undesirable because it necessitates complex design, where equipment and material erosion become the main challenge. In general, there are two types of fluidized beds: traditional and pulsed. Pulsed fluidized beds have two periods of activity and inactivity, with gas entering the bed only during the inactive periods. A new type of pulsed fluidized bed was proposed by Coppens & Ommen (2002). They combined steady and pulsed flow (combined flow) in a sinusoidal pattern to experimentally achieve improved hydrodynamic behaviors in fluidized beds. They observed the regular bubble patterns at a pulse frequency of 2-7 Hz. Additionally, new types of chaos-to-order transitions were achieved by utilizing combined flow.

Li et al (2020b) utilized combined flow in a sinusoidal pattern ($U(t) = (U_C + U_P) + U_P \sin(2\pi ft)$) to investigate the hydrodynamic behavior of a pulsed fluidized bed.

Where U_p and U_c are pulsed and steady gas velocities, respectively, and f is the pulse frequency. They pointed out that particles exhibited regular motion, and the mixing effect of particles was enhanced by increasing the pulse frequency. Oliveira et al. (2020) numerically studied the effect of mean gas velocities and the oscillation amplitude at 3.5 Hz in a sinusoidal pattern ($V = V_{mf}(V_M + V_A \sin(2\pi f t))$). V_{mf} is the minimum fluidization velocity, V_M the is temporal average gas velocity, V_A is the oscillation amplitude, and f is the pulse frequency. Results showed that by increasing V_A, the system transitioned from a bubbling regime to a state where a void layer formed at the bottom of the bed. Under $V_M = 1.1$, fluidization improved due to the formation of highly stable bubbles.

Studies on the combination of steady and pulsed flow (combined flow) are rather scarce, and the sinusoidal pattern used is not cost-effective due to the need for complex equipment. Due to the rapid change in gas velocity from zero to a defined value under high pulse frequency conditions, high-pressure fluctuations occur, leading to serious damage to materials and equipment. The impact of different velocity ratios of steady to pulsating flow surges on bed hydrodynamics is unclear.

The main goal of this article is to conduct a numerical investigation of combined flow pulsation, specifically examining a rectangular pulsating flow superimposed on a continuous steady flow in a fluidized bed. The study examines the effects of the ratio of velocity pulsation amplitude to the continuous velocity on bed hydrodynamic parameters. It was hypothesized that maintaining a steady flow and superimposing pulsations in a rectangular pattern may facilitate fluidization with appropriate quality at very low pulse frequencies. Computational fluid dynamic (CFD) was used in the present study to simulate the 2D pulsed fluidized bed. The focus was on the quality of fluidization across a wide range of frequencies, from 0.05 Hz to 10 Hz. The study also investigated the effect of various steady airflow velocities ranging from U_{mf} to $3U_{mf}$ during a period of inactivity in a rectangular pattern, where pulsed flow is not present while maintaining a consistent temporal average gas flow velocity. The hydrodynamics and fluidization behavior of the bed were examined, including temporal average bed pressure drop, solid volume fraction, bed expansion ratio, and fluidization index.

2. THE GOVERNING EQUATIONS

Two-fluid model was used in this investigation. The governing equations are introduced in this section.

The continuity equation for each phase is represented by Equation (1):

$$\frac{\partial}{\partial t}(\alpha_i \rho_i) + \nabla(\alpha_i \rho_i u_i) = 0 \tag{1}$$

Where i=p is for particles and i=q is for fluid phase, α_i and ρ_i represent the volume fraction and density of phase i, respectively.

Momentum conservation equations for the fluid and solid phases are presented in Equations (2) and (3), respectively (Mostafaei et al., 2020)

$$\frac{\partial}{\partial t}(\alpha_q \rho_q u_q) + \nabla(\alpha_q \rho_q u_q^2) = -\alpha_q \nabla p + \nabla \overline{\overline{\tau}}_q + \alpha_q \rho_q g + R_{qp} \tag{2}$$

$$\frac{\partial}{\partial t}(\alpha_p \rho_p u_p) + \nabla(\alpha_p \rho_p u_p^2) = -\alpha_p \nabla p - \nabla p_p + \nabla \overline{\overline{\tau}}_p + \alpha_p \rho_p g + R_{pq} \tag{3}$$

Where $\alpha_p + \alpha_q = 1$. $\overline{\overline{\tau}}_p$ is Reynolds stress tensor defined by Equation (4).

$$\overline{\overline{\tau}}_p = \alpha_p \mu_p (\nabla u_p + \nabla u_p^T) + \alpha_p \left(\lambda_p - \frac{2}{3}\mu_p\right) \nabla u_p I \tag{4}$$

The solid pressure P_p, solid shear viscosity μ_p, and solid bulk viscosity λ_p are defined in 2.1.

Interphase momentum exchange is expressed by Equation (5).

$$R_{pq} = -R_{qp} = K_{pq}\left(u_p - u_q\right) \tag{5}$$

2.1. Constitutive Equations

Based on Lun et al. (1984) theory of granular kinetics, initially, the average granular energy decreases into kinetic energy due to the fluctuations of randomly moving particles, and then transforms into heat as a result of inelastic collisions. The granular temperature is defined by Equation (6):

$$\Theta_p = \frac{c^2}{3} \tag{6}$$

Where c represents the component of the fluctuating solid velocity. The granular temperature of the solid phase is determined by the kinetic energy resulting from particles moving randomly. The granular temperature of the solid phase is governed by Equation (7) (Wachem et al., 1998):

$$\frac{3}{2}\left[\frac{\partial}{\partial t}(\rho_p \alpha_p \Theta_p) + \nabla.(\rho_p \alpha_p u_p \Theta_p)\right] = (-p_p \overline{\overline{I}} + \overline{\overline{\tau}}_p) : \nabla u_p + \nabla.(k_{\Theta_p} \nabla \Theta_p) - \gamma_{\Theta_p} + \varphi_{qp} \tag{7}$$

Where Θ_p is the granular temperature. The first term on the right-hand side of Equation (7) represents the energy generation by the solid stress tensor; the second term denotes the diffusion of energy, the third term shows the dissipation of energy, and the last term introduces the energy exchange between two phases.

Diffusion coefficient is defined by Equation (8) (Syamial & O'Brien, 1989):

$$k_{\Theta p}=\frac{75\rho_p d_p(\Theta_p\pi)^{0.5}}{192(1+e_{pp})g_{0,pp}}\left[1+1.2\alpha_p g_{0,pp}(1+e_{pp})\right]^2 \quad (8)$$
$$+2\rho_p\alpha_p^2 d_p(1+e_{pp})g_{0,pp}(\frac{\Theta_p}{\pi})^{0.5}$$

Where e_{pp} shows restitution coefficient for particle collision.

In equation (7), by considering the steady-state condition of granular energy and local dissipation, the equation of granular temperature can be expressed as an algebraic equation by neglecting the terms of diffusion and convection. The algebraic equation is defined as:

$$0=(-\nabla.p_p\bar{\bar{I}}+\bar{\bar{\tau}}_p):\nabla u_p-\gamma_{\Theta_p} \quad (9)$$

The collisional dissipation of energy, γ_{Θ_p}, represents the rate at which energy is dissipated in the solid phase when particles collide with each other. This term is defined as (Lun et al., 1984):

$$\gamma_{\Theta m}=\frac{12(1-e_{pp}^2)g_{0,pp}}{d_p\sqrt{\pi}}\rho_p\alpha_p^2\Theta_p^{1.5} \quad (10)$$

Particle pressure is obtained by Equation (11) (Gidaspow et al., 1992):

$$P_p=\alpha_p\rho_p\Theta_p+2\rho_p(1+e_{pp})\alpha_p^2 g_0\Theta_p \quad (11)$$

Where g_0 is a radial distribution function.

The radial distribution function is defined by Equation (12) (Ogawa et al., 1980):

$$g_{0,pp}=\left[1-(\frac{\alpha_p}{\alpha_{p,\max}})^{\frac{1}{3}}\right]^{-1} \quad (12)$$

Where $\alpha_{p,\max}$ is the maximum solid packing limit.

The solid stress tensor consisted of collisional, kinetic, and the frictional parts.

$$\mu=\mu_{p,col}+\mu_{p,kin}+\mu_{p,fr} \quad (13)$$

The collisional part of the shear viscosity is (Bizhaem & Tabrizi, 2017; Gidaspow et al., 1992):

$$\mu_{p,col}=0.8\alpha_p\rho_p d_p g_{0,pp}(1+e_{pp})\left(\frac{\Theta_p}{\pi}\right)^{0.5} \quad (14)$$

The kinetic viscosity is defined by Syamlal et al. (Syamlal et al., 1993; Ghadirian & Arastoopour, 2016):

$$\mu_{p,kin}=\alpha_p\rho_p d_p\frac{\sqrt{\theta\pi}}{63-e_{pp}}\left[1+\frac{2}{5}(1+e_{pp})(3e_{pp}-1)\alpha_p g_{0,pp}\right] \quad (15)$$

The solid bulk viscosity is expressed as (Ding and Gidaspow 1990):

$$\lambda_p=\frac{4}{3}\alpha_p\rho_p d_p g_{0,pp}(1+e_{pp})\left(\frac{\Theta_p}{\pi}\right)^{0.5} \quad (16)$$

The frictional viscosity is defined by Schaeffer equation (Schaeffer 1987):

$$\mu_{p,fr}=\frac{p_p\sin\phi}{2(\mathrm{I}_{2D})^{0.5}} \quad (17)$$

I_{2D} denotes the second invariant of the deviatory stress tensor. ϕ is the internal friction angle and p_p is pressure of particles.

2.2. Drag Model

Symalal-O'Brein, which is well-known in fluidization modeling (Bizhaem & Tabrizi, 2017), was used for momentum exchange between phases.

$$R_{qp}=\frac{3\alpha_p\alpha_q\rho_q}{4u_{r,p}^2 d_p}C_D\left(\frac{\mathrm{Re}_p}{u_{r,p}}\right)\left|u_p-u_q\right| \quad (18)$$

The drag coefficient, C_D, and Reynolds number, Re_p, were calculated by Equations (19) and (20), respectively:

$$C_D=(0.63+\frac{4.8}{\sqrt{\mathrm{Re}_p/u_{r,p}}})^2 \quad (19)$$

$$\mathrm{Re}_p=\frac{\rho_q d_p\left|u_p-u_q\right|}{\mu_q} \quad (20)$$

3. SIMULATION METHOD

The two-dimensional model was chosen for simulations under transient conditions due to its shorter computational time while maintaining high accuracy. The properties of gas and solid phases, bed geometry, pulsed flow parameters, grid number, and time step for simulations are listed in Table 1. The governing equations described in sections 2.1 and 2.2 were solved using the finite volume method implemented in the software. The PC-SIMPLE algorithm is chosen for coupling pressure and velocity. The on-off pulsed and combined airflow velocities were defined in the CFD code (using ANSYS Fluent 17.0 software) through user-defined functions (UDF). The second-order upwind method was defined for all the convection equations. A time step of 10^{-5} s, with 85 iterations per time step, was defined to achieve convergence. All of the residual variables were set at 0.001. The results were reported after 5 s to avoid the effects of simulation initiation. The total duration of the simulation was 20 s and the time average of variables was considered from 5 s to 20 s. In this article, the bed expansion ratio and fluidization index were used to analyze the effect of different airflow types on fluidization quality. The bed expansion ratio is defined by Equation (20) (Reuge et al. 2008):

$$\text{Bed expansion ratio} = \frac{H_{\max}}{H_{static}} \quad (20)$$

Where H_{static} and H_{max} represent the static and maximum bed height during fluidization, respectively.

The fluidization index is defined by Equation (21) (Köksal & Vural, 1998):

Table 1 Different parameters used in these simulations

Parameters	Values
Gas density (ρ_q)	1.225 (kg/m^3)
Gas viscosity (μ_q)	1.789×10^{-5} (kg/m.s)
Temporal average superficial gas velocity	0.1 (m/s)
Minimum fluidization velocity (U_{mf})	0.021 (m/s)
Velocity in an inactive period (u_{steady})	0, U_{mf}, $2U_{mf}$, $3U_{mf}$
Solid diameter (d_p)	196 (μm)
Solid density (ρ_p)	2550 (kg/m^3)
Maximum solid packing limit ($\alpha_{p,\,max}$)	0.63
Initial solid packing (α_{p0})	0.6
Restitution coefficient (e_{pp})	0.9
Bed diameter (D)	0.11 (m)
Bed height (H)	0.5 (m)
Initial static bed height (H0)	0.15 (m)
Pattern	Square
Frequency (f)	0.05,0.1,0.5,1,4,10 Hz
Velocity at on-period (U_P)	0.2,0.179, 0.158,0.137 (m/s)
Grid number	13750
Time step (Δt)	10^{-5} (s)

$$FI = \frac{\Delta P_{max}}{W\ /A} \tag{21}$$

Where ΔP_{max}, W , and A represent the maximum bed pressure drop, particle's weight, and the cross-sectional area of the bed, respectively.

4. BED GEOMETRY

Figure 1 shows the schematic of the simulated geometry of the fluidized bed. A cylindrical bed with an internal diameter of 11 cm and a height of 50 cm was used in this investigation. Silica and air were selected as the solid and fluid phases, respectively. Spherical silica seed particles used to fill the bed had a uniform diameter of 196 μm and a density of 2550 kg/m³. The static bed height was 15 cm. ANSYS Fluent 17.0 software was used to create the bed geometry and generate grids for the numerical study.

5. BOUNDARY AND INITIAL CONDITIONS

a. Gas Flow Pulsation

Airflow enters uniformly at the bottom of the bed. Additionally, the initial velocity was set to zero in the bed.

Three categories were investigated for gas flow in the bed.

1. Steady Airflow: Air enters the bed continuously at a constant velocity.
2. On-off pulsed flow of gas: Airflow is turned on for a period and then turned off. The cycle is repeated.

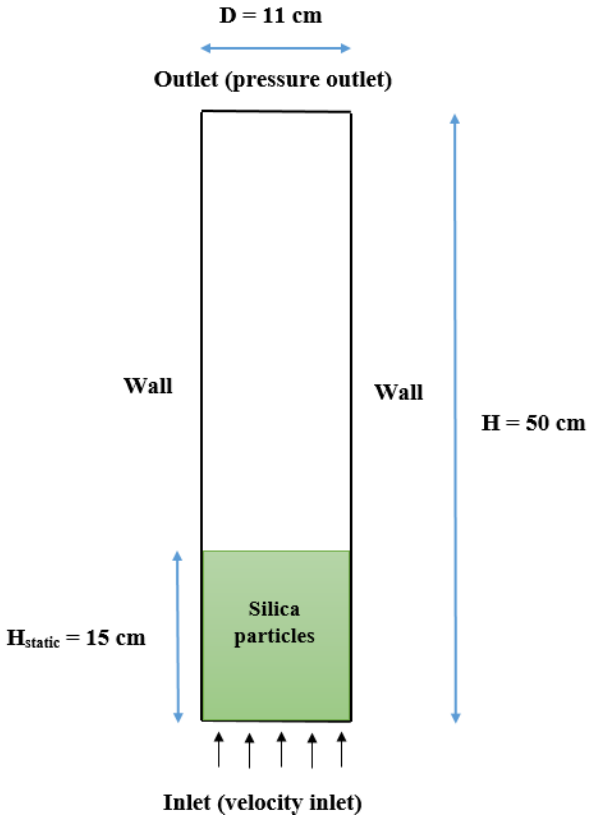

Fig. 1 Simulated domain of pulsed fluidized bed

3. Combined airflow: A constant base airflow is always present, with on-off airflow added to the base flow.

b. Particle Phase

The particle velocity was set to zero at the inlet. The initial solid packing was patch 0.6 (Bizhaem & Tabrizi, 2017) at a static bed height of 15 cm, and at the inlet, it was set to zero. The outlet boundary condition was defined based on the flow pressure (pressure outlet) at the outlet with a zero value.

c. wall Region

For each phase, the wall boundary condition was set to zero (Oliveira et al., 2020). The stationary wall and no-slip conditions were considered as wall boundary conditions for both gas and solid phases.

For all three cases introduced in 5-a, the temporal average velocity was kept constant at 0.1 m/s, which was 4.67 times the minimum fluidization velocity. Various pulsation schemes were examined in this paper, as outlined in Table 2.

6. GRID INDEPENDENCY

The temporal average solid volume fraction for an 11 cm diameter and 50 cm height pulsed fluidized bed at 0.05 Hz for different grid sizes is depicted in Fig. 2. The maximum and average solid volume fractions have deviated by 3% and 1%, respectively. Since the results are independent of the number of grids, the remaining numerical calculations were conducted at 13750.

Table 2 Different inlet airflow types

Run	1	2	3	4	5
u_{steady} (m/s)	0.1	0	0.021	0.042	0.063
u_{pulsed} (m/s)	0	0.2	0.158	0.116	0.074
Velocity at on-period (U_p) (m/s)	-	0.2	0.179	0.158	0.137
Temporal average velocity on cycle (m/s)	0.1	0.1	0.1	0.1	0.1
Velocity ratio (U_p/U_{mf})	0	9.52	8.52	7.52	6.52

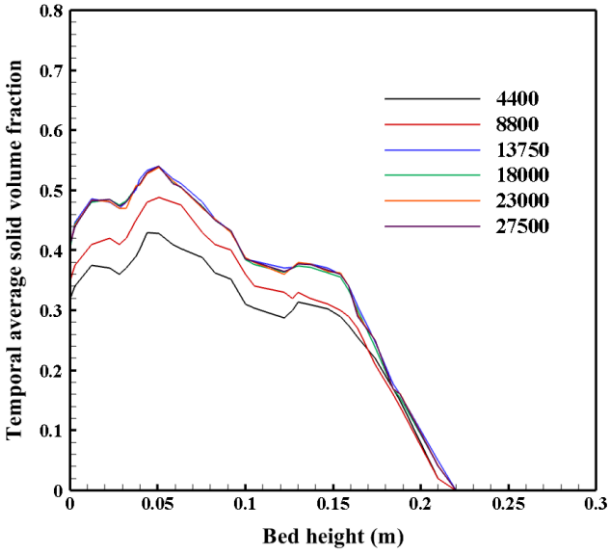

Fig. 2 Effect of cells numbers on temporal average solid volume fraction

7. VALIDATION

To validate the simulated model, a comparison was made between the published experimental data (Bizhaem & Tabrizi, 2013) and the simulation results presented in this paper. The comparison was carried out using a fluidized bed with a diameter of 11 cm and a height of 50 cm. The particles with average diameters of 95 μm and 196 μm were used for fluidization by airflow. Simulations were performed under steady and pulsed airflow conditions at a 10 Hz pulse frequency and a 15 cm static bed height. Figure 3 illustrates a comparison between experimental data and our simulation results for pressure drop versus velocities exceeding the minimum fluidization velocity under steady airflow and a 10 Hz pulse frequency for particles with a diameter of 196 μm. The maximum deviations under conditions of steady airflow and pulsed airflow were 6% and 8%, respectively. Figure 4 illustrates a comparison between experimental and numerical results of solid volume fraction with changes in bed height under pulsed airflow at 1 Hz for 95 μm particle diameter. It can be seen that our results are in good agreement with the published experimental results.

8. RESULTS AND DISCUSSION

All results are presented at a temporal average airflow velocity of 0.1m/s, indicating a constant amount of air injected into the bed during the cycle. In this section, the

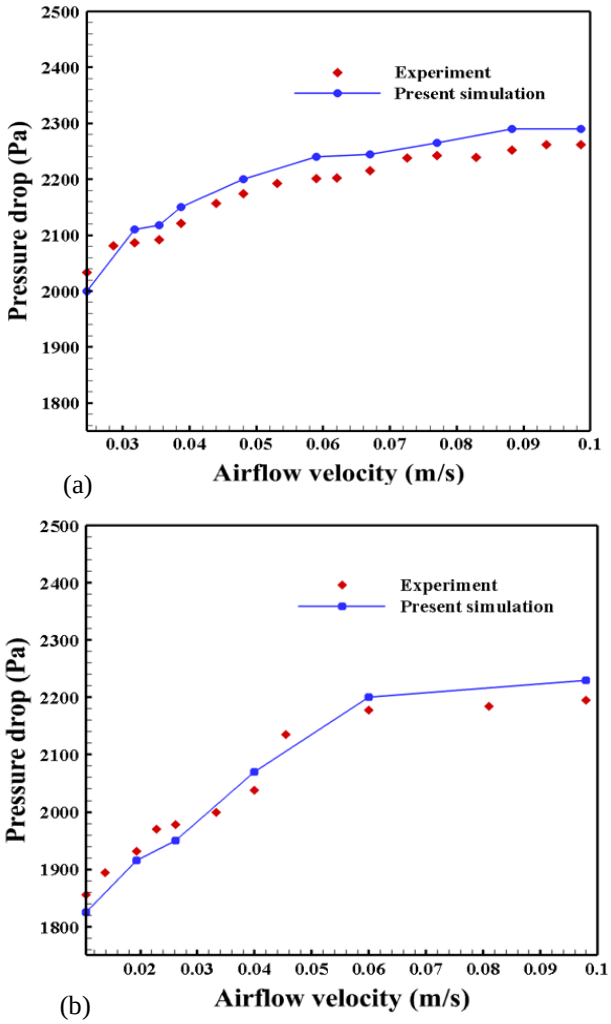

Fig. 3 Comparison of experiment results (Bizhaem & Tabrizi, 2013) and our simulation pressure drop under (a) steady airflow and (b) 10 Hz pulse frequency

behavior of bed pressure drop, bubble generation, bed expansion ratio, and fluidization index were investigated at various steady airflow velocities combined with pulsed airflow.

8.1. Pressure Drop

At first, the pressure drop was investigated under conditions of steady airflow (no pulsation) and then with pulsed airflow at a pulse frequency of 0.05-10 Hz. The pressure drop of steady airflow is approximately 2200 Pa, which is equivalent to the weight of the bed materials per unit cross-sectional area of the bed. Under pulsed airflow

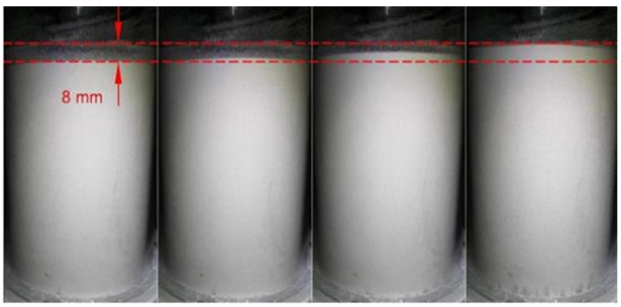

(a) Experiment result (Bizhaem & Tabrizi, 2013)

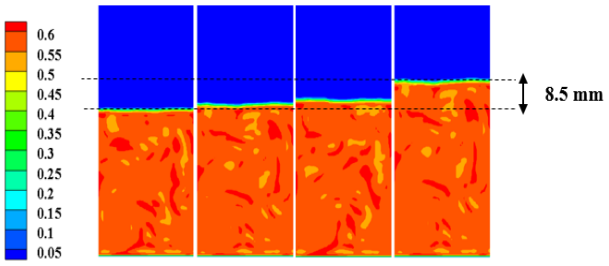

(b) Our numerical result

Fig. 4 Comparison of (a) experiment (Bizhaem & Tabrizi, 2013) and (b) our numerical results of solid volume fraction and bed height changes

conditions, with an increase in pulsation up to 10 Hz, the pressure drop decreased to approximately 2200 Pa. This reduction was attributed to the decrease in inactive periods and the enhancement of particle mixing. This behavior is related to the uniform distribution of particles in the bed, which directly affects the bed pressure drop because the gas can easily move through the particles in the bed.

The pressure drop at frequencies other than 0.1, 0.5, 1, and 4 Hz deviates significantly from 2200 Pa due to particle collapse during extended inactive periods and bed transitions to a packed state.

Figure 5 illustrates the effect of various steady airflow velocities ranging from U_{mf} to $3U_{mf}$ (equivalent to velocity ratios of 8.52 to 6.52, respectively) on bed pressure drop at pulse frequencies ranging from 0.05 Hz to 10 Hz under combined airflow conditions.

Under combined airflow at all ratios, the slope of the pressure drop initially increases and then tends to decrease with increasing pulse frequency up to 10 Hz. At low frequencies (0.05 Hz and 0.1 Hz), the duration of an inactive period is longer compared to the other frequencies (0.1, 0.5, 4, and 10 Hz). Therefore, introducing a steady airflow during this period has a greater impact on pressure drop by preventing the complete collapse of particles in the bed. At a velocity ratio of 6.52, no significant changes in pressure drop were observed across frequencies ranging from 1 Hz to 10 Hz due to a shorter inactive period.

Reduction in velocity ratios from 8.52 to 6.52 (equivalent to U_{mf} to $3U_{mf}$ in steady airflow velocity) would increase bed pressure drop, particularly at very low frequencies from 0.05 Hz to 0.5 Hz. These changes were significantly reduced under conditions below 10 Hz. It has been determined that at very low pulse frequencies, by

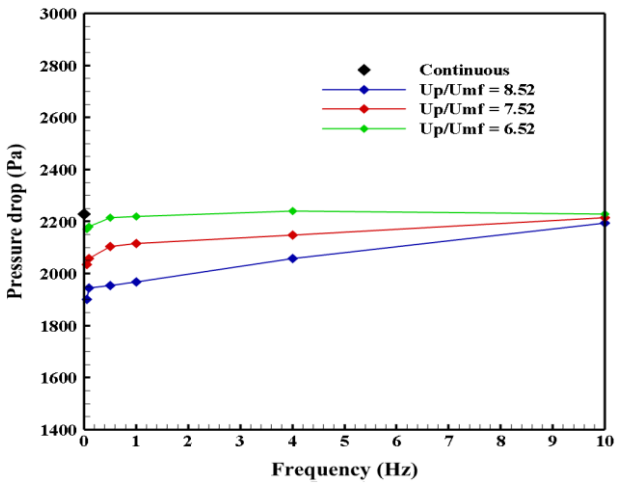

Fig. 5 Pressure drop versus different pulse frequencies under steady and combined airflow at different velocity ratios

adding and increasing steady airflow velocity (combined flow) up to $3U_{mf}$ (velocity ratio 6.52), the bed pressure drop tended to be nearly close to the steady airflow value of 2200 Pa. This is done to prevent particles from stopping and accelerating, to ensure they return to the bottom of the bed, and to guarantee a uniform distribution of particles. The maximum change in pressure drop is observed at a velocity ratio of 6.52 compared to 9.52 at 0.05 Hz, corresponding to approximately 27%. At 10 Hz, this change is 4.5%.

8.2. Bubble Generation

For a better understanding of the effect of combined airflow on solid volume fraction at different velocity ratios, snapshots under various gas flow conditions are provided. Due to space limitations, we provide the number of snapshots at very low (0.05 Hz), medium (1 Hz), and high (10 Hz) pulse frequencies.

Solid volume fraction contours under only steady and pulsed airflow in one cycle of pulsation are displayed in Fig. 6. Under steady airflow (Fig. 6(a)), large bubbles formed and moved upward along the height of the bed. As shown in Fig. 6, increasing the pulse frequency from 0.05 Hz to 10 Hz resulted in a significant reduction in the size of bubbles. This was attributed to the shorter duration of two periods and a lower amount of airflow entering the bed. Based on the snapshots of solid volume fraction, an increase in pulse frequency resulted in smaller bubble sizes and higher particle concentrations. This led to improved bed uniformity and fluidization quality by supplying the necessary air to fluidize particles. This behavior has been reported in other experimental and numerical studies (Köksal & Vural, 1998; Liu et al., 2016). Also, by comparing Figs. 6(b) and (d), it is observed that the majority of changes in bed height have occurred at very low frequencies.

Figure 7 depicts snapshots of the solid volume fraction and velocity profile under combined airflow at different velocity ratios of 8.52 ($u_{steady} = U_{mf}$), 7.52 ($u_{steady} = 2U_{mf}$), and 6.52 ($u_{steady} = 3U_{mf}$). The snapshots were taken at one pulsation cycle, during which the active and inactive

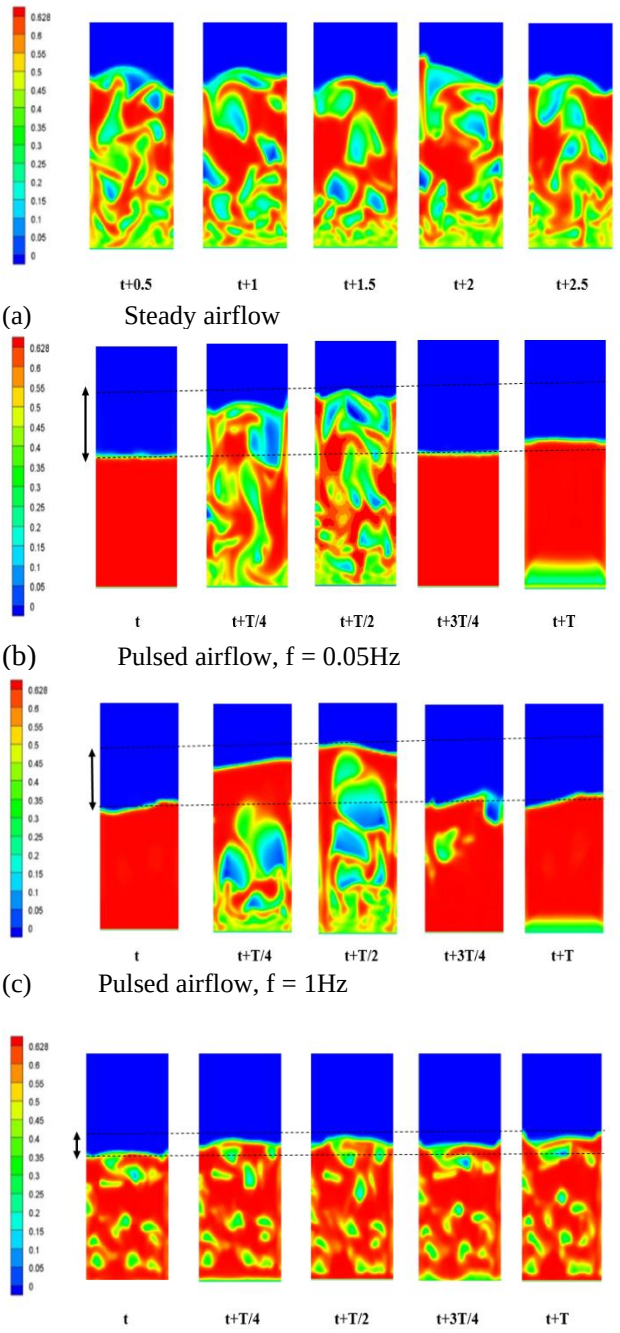

(a) Steady airflow

(b) Pulsed airflow, f = 0.05Hz

(c) Pulsed airflow, f = 1Hz

(d) Pulsed airflow, f = 10Hz

Fig. 6 Bubble formation under condition of steady and one period of only pulsed airflow

periods lasted from t to t+T/2 and t+ T/2 to t+T, respectively. Comparing Fig. 6(b) and Fig. 7(a), it can be observed that the entrance of steady airflow during the cessation of pulsed flow had a notable impact on the size of the bubbles at a frequency of 0.05 Hz. Smaller bubbles were also observed in the 8.52 velocity ratio compared to only steady and pulsed flow (Figs. 6(a) and 6(b)). When the velocity ratio was 9.52 (with only pulsation (u_{steady} =0)), the size of the bubble was the largest, and it decreased as the velocity ratio decreased to 6.52. Upon increasing the steady airflow velocity (resulting in a decrease in velocities ratio), the amount of airflow entering in two periods decreased. As a result, the changes in bed height also decreased due to the improved fluidization uniformity.

These results were also observed when the pulse frequency was 1 Hz. The effect of velocity ratio was much greater at very low frequencies due to a longer inactive period. Figure 7(c) shows that at a pulse frequency of 10 Hz, no obvious effect was observed on bed hydrodynamics by adding steady airflow during an inactive period. This is due to the very short duration of the two periods and the insufficient air supply needed to create larger bubbles. At 10 Hz, the number of bubbles at the bottom of the bed is higher than at the top due to the initial high amount of air injection at the bottom. The air then spreads throughout the bed, causing the bubbles to rise, combine, and eventually exit the bed.

Bubble size plays a crucial role in the quality of fluidization as it significantly influences bed homogeneity and particle concentration. The results show that achieving high fluidization quality is possible by increasing particle concentration, which results in a smaller bubble size and a more uniform solid volume fraction, as well as pressure drop. Additionally, an increase in pulse frequency can be achieved at very low frequencies by introducing steady airflow during an inactive period (combined flow).

8.3. Comparison of Three Airflow Types

In this section, a comparison was conducted on the effect of three types of airflow – steady airflow only, on-off pulsed airflow, and combined airflow – at various velocity ratios on fluidization quality. In the pulsed fluidized bed, the investigation of fluidization quality could be studied by different important parameters such as bed pressure drop, solid volume fraction, particle concentration, bed expansion ratio, and fluidization index. In this section, the quality of bed fluidization was investigated using the bed expansion ratio and fluidization index as dimensionless parameters.

8.3.1. Bed Expansion Ratio

The maximum height of the fluidized bed was measured at a solid volume fraction of 0.02 in this study. A larger bed expansion ratio is attributed to the larger size of bubbles and weaker bed stability, resulting in lower fluidization quality. The parameters of flow type, pulse frequency, and gas velocity have a greater effect on the bed expansion ratio.

For a better understanding of the effect of combined flow on bed expansion ratio, the study focuses on the impacts of a wide range of pulse frequencies (0.05 Hz-10 Hz) and flow types, including pulsed and combined airflow, while keeping the other parameters constant. Figure 8 illustrates the effect of pulsed airflow alone (9.52 velocity ratio) and combined airflow (8.52, 7.52, and 6.52 velocity ratios) on bed expansion ratio at various pulse frequencies. As the pulse frequency increases from 0.05 Hz to 10 Hz, the duration of the two mentioned periods decreases, along with the expansion ratio and bubble size (Fig. 6). The simulation results are in agreement with Zhang and Koksal (2006) and Bizhaem and Tabrizi (2017), respectively.

At a pulse frequency of 0.05 Hz, the maximum bed expansion value is related to a ratio of 9.52. This is due to the formation of large bubbles throughout the bed and an

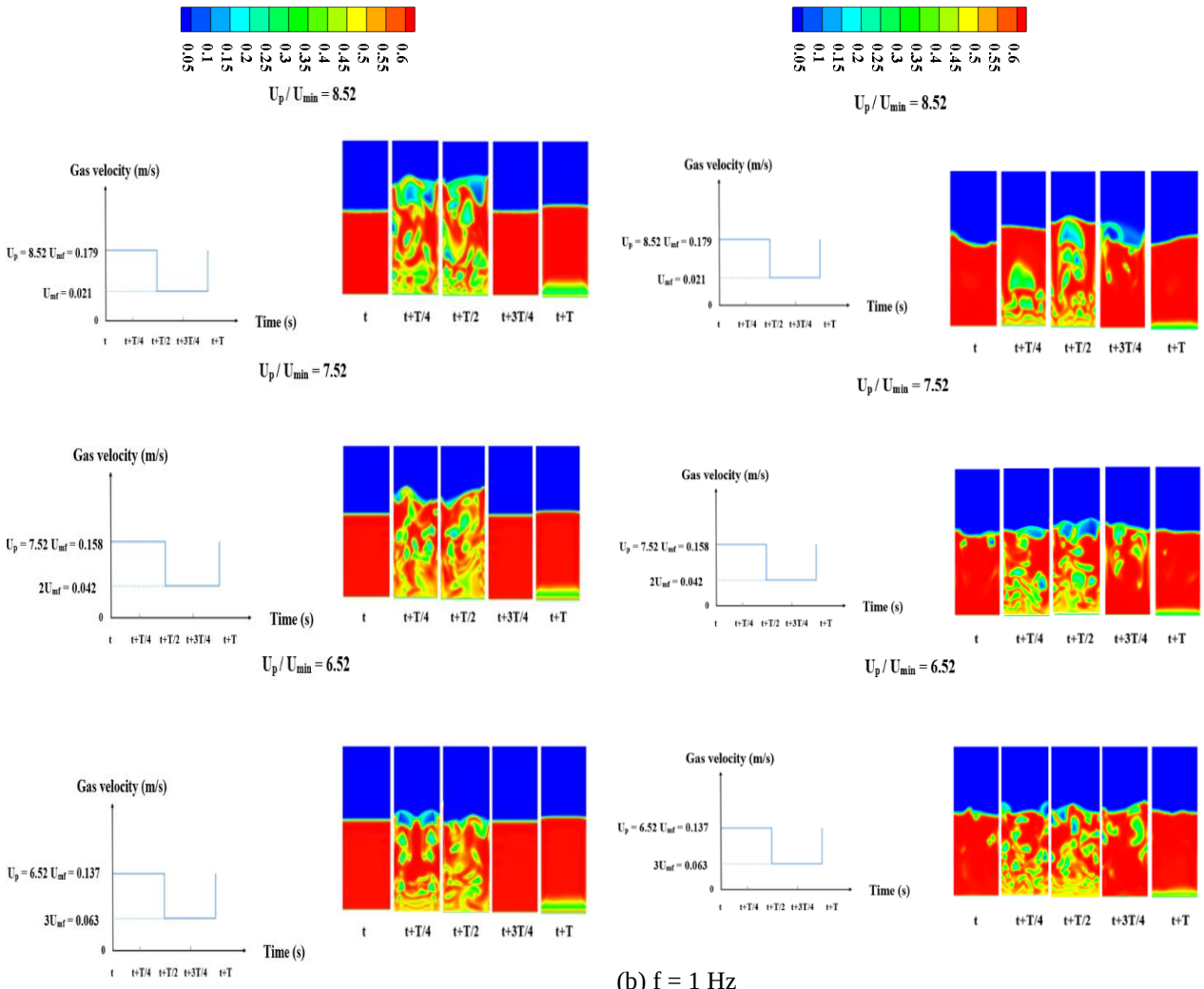

(a) f = 0.05 Hz

(b) f = 1 Hz

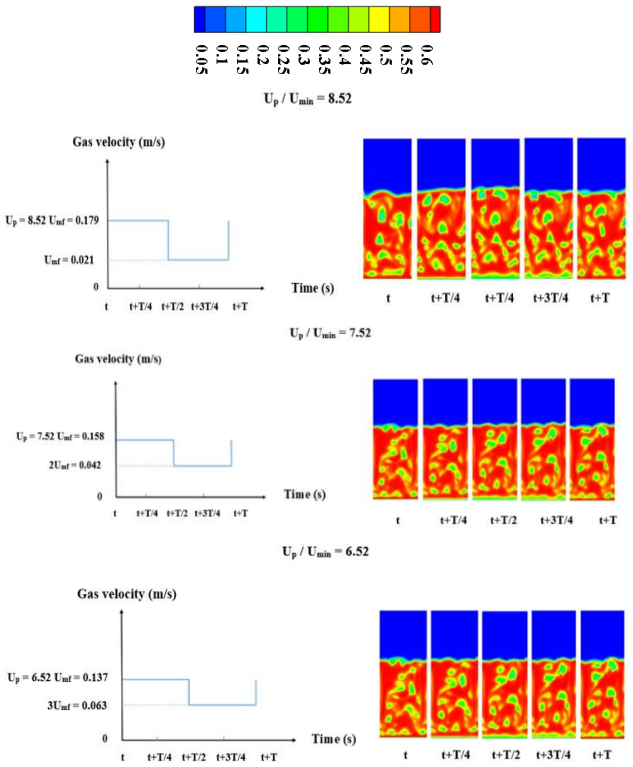

(c) f = 10 Hz

Fig. 7 Solid volume fraction contours in different velocity ratios at 0.05, 1, and 10 Hz pulse frequencies

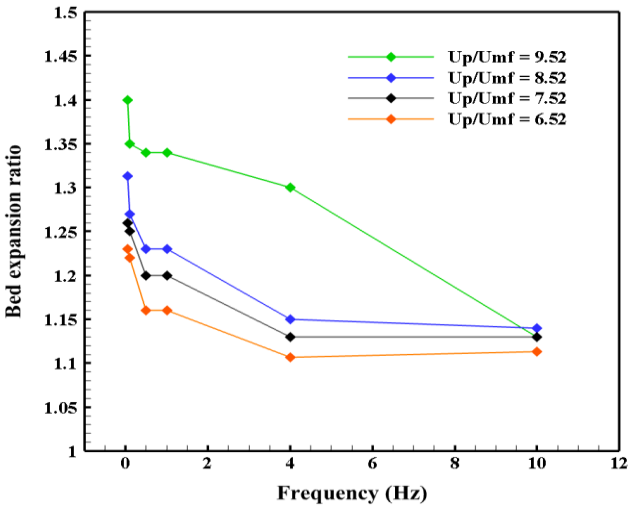

Fig. 8 Effects of different airflow types on bed expansion ratio versus pulse frequencies of 0.05 Hz to 10 Hz

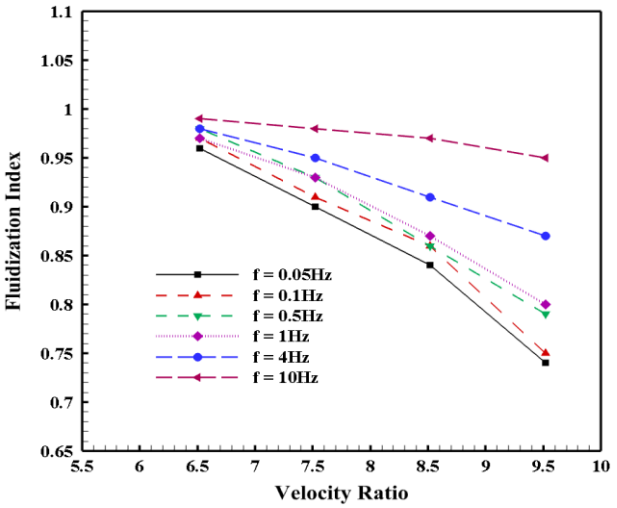

Fig. 9 Effect of different airflow types on fluidization Index versus different velocity ratios of 9.52, 8.52, 7.52, and 6.52

increase in fluidization height, where no steady airflow exists. Considering steady airflow during an inactive period (combined flow) and increasing its velocity to $3U_{mf}$ (reducing the velocity ratio to 6.52), at all pulse frequencies causes a reduction in bed expansion ratio because the required air to fluidize particles is supplied. Therefore, by increasing the uniform distribution of particles, the bed expansion ratio decreases.

The significant effect of a decrease in velocity ratio on bed expansion ratio was particularly noticeable at very low pulse frequencies, especially at a frequency of 0.05 Hz, where it reached approximately 21%. This was attributed to a longer inactive period, which prevented the complete collapse of particles. At a frequency of 10 Hz, when the velocity ratio is changed to 7.52, the bed expansion ratio remains at 1.2. At a lower velocity ratio of 6.52, the bed expansion ratio decreases to 1.1. Although a smaller value was obtained at a frequency of 10 Hz compared to the other frequencies due to the injection of high-velocity steady airflow during an inactive period at very low frequencies, the bed expansion ratio reaches a value almost near that of the high frequency, and fluidization quality improves.

At very low frequencies, the duration of the two periods is long. Due to the complete collapse of particles and the formation of large bubbles, as shown in Figure 6, the bed expansion ratio increases, while fluidization quality decreases. Upon introducing a steady airflow during an inactive period to prevent particle collapse, the bubble size decreased, resulting in a decrease in the bed expansion ratio. At high frequencies, due to shorter periods, the introducing of steady airflow did not significantly affect the size of bubbles. As a result, bed expansion did not change significantly, and the distribution of particles remained uniform.

8.3.2. Fluidization Index

The fluidization index indicates the fluidization behavior and quality of a pulsed fluidized bed. When this parameter approaches a value of one, fluidization quality is high, and the bed is fully developed. This indicates a high degree of uniformity in bed expansion and particle distribution (Namdarkedenji et al 2018).

Figure 9 displays the effect of various airflow types on fluidization quality across a wide range of pulse frequencies from 0.05 Hz to 10 Hz at different velocities. Under pulsed airflow alone, at a high frequency of 10 Hz, the fluidization index was also high, reaching approximately 1 due to the enhanced uniformity in particle distribution and shorter intervals between periods. At a frequency of 0.05 Hz, the fluidization index was 0.72, indicating poor fluidization. This is because the necessary air is not supplied to fluidize particles due to the long inactive period and complete settling of particles.

It can be seen that at a 9.52 velocity ratio (only pulsed airflow), the difference between the fluidization index at low and high frequencies was far higher than the ratio of 6.52 due to a reduction in bubble size and bed uniformity. Therefore, the bed expansion ratio decreases when the pulsed frequency increases to 10 Hz because by reducing the amount of air injected in an active period helps maintain the fluidization state.

Under combined airflow, when decreasing the velocity ratios from 8.52 to 6.52, the graphs showed an almost linear relationship at frequencies ranging from 0.05 to 4 Hz. The slope of the graphs decreased as the frequency increased to 10 Hz, attributed to the shorter inactive period and smaller bubble size. At very low frequencies (0.05 Hz – 0.5 Hz), when steady airflow is introduced during an inactive period at a velocity ratio of 6.52 ($3U_{mf}$ velocity), the FI approaches a value close to 10 Hz frequency (a value of one) under only pulsation because the increase in solid volume fraction at lower velocity ratios results in greater bed uniformity and a reduction in bubble size.

It was found that achieving suitable fluidization quality is possible at all frequencies, especially at very low frequencies, by combining airflow at a velocity equal to the coefficients of U_{mf} during an inactive period. Additionally, an increase in the steady airflow velocity

during an inactive period leads to achieving a higher fluidization index. The fluidization index increases by about 32% and 2% when the velocity ratio is decreased from 9.52 to 6.52 at frequencies of 0.05 Hz and 10 Hz, respectively.

9. CONCLUSIONS

2D-pulsed fluidized bed hydrodynamics were studied using the Eulerian-Eulerian method in conjunction with KTGF for silica particles with a diameter of 196 µm. Pulsation combines airflow with varying amplitudes while maintaining a constant temporal average gas velocity to enhance fluidization quality at lower pulse frequencies. The following conclusions can be drawn from the present study:

- By combining pulsed and steady airflow, improved fluidization quality was achieved within the frequency range of 0.05–1 Hz. This improvement can be attributed to a decrease in bubble size and bed expansion ratio. Furthermore, by preventing the collapse of particles, greater bed uniformity is achieved. In contrast, for the pulsed flow without steady flow at the same temporal average gas velocity, the quality at these frequencies was poor due to non-uniform particle distribution, higher bed expansion ratio, and larger bubble size. Thus, the best quality was achieved at a frequency of 10 Hz.
- Upon increasing the pulse frequency to 10 Hz, the effects of combined airflow at various velocities on the bed hydrodynamics and fluidization quality were found to be insignificant. Combined airflow revealed significant effects on the quality of fluidization quality at low frequencies.
- In the present study, with a temporal average gas velocity of 0.1 m/s, the optimal velocity ratio of pulsed to steady airflow velocities, as a significant parameter affecting fluidization quality, was found to be within the range of 2.76–1.17.

ACKNOWLEDGEMENTS

The authors are grateful for the financial support provided by the Iran National Science Foundation (INSF, Grant no 98003159) for this project.

CONFLICT OF INTEREST

No conflict of interest

AUTHORS CONTRIBUTION

Naghmeh Abedi: Conceptualization (equal); Formal analysis (equal); Investigation (equal); Software (lead); Validation (lead); Writing – original draft (lead); **Mohsen Nasr Esfahany:** Conceptualization (equal); Formal analysis (equal); Investigation (equal); Funding acquisition (supporting); Project administration (supporting); Supervision (supporting); Writing – review & editing (supporting).

REFERENCES

Bizhaem, H. K., & Tabrizi, H. B. (2013). Experimental study on hydrodynamic characteristics of gas – solid pulsed fl uidized bed. *Powder Technology*, *237*, 14–23. https://doi.org/10.1016/j.powtec.2013.01.001

Bizhaem, H. K., & Tabrizi, H. B. (2017). Investigating effect of pulsed flow on hydrodynamics of gas-solid fluidized bed using two- fluid model simulation and experiment. *Powder Technology*, *311*, 328–340. https://doi.org/10.1016/j.powtec.2017.01.027

Coppens, M. & Ommen, J. R. Van (2003). *Structuring chaotic fluidized beds. Chemical Engineering Journal, 96, 117-124. https://doi.org/10.1016/j.cej.2003.08.007*

de Oliveira, D. G., Wu, C. L., & Nandakumar, K. (2020). Numerical investigation of pulsed fluidized bed using CFD-DEM: Insights on the dynamics. *Powder Technology*, *363*, 745–756. https://doi.org/10.1016/j.powtec.2020.01.016

Di Nardo, A., Calchetti, G., & Stendardo, S. (2018). Modeling and simulation of an oxygen-blown bubbling fluidized bed gasifier using the computational particle-fluid dynamics (CPFD) approach. *Journal of Applied Fluid Mechancis, 11*(4), 825–834. https://doi.org/10.29252/jafm.11.04

Ding, J., & Gidaspow, D. (1990). A bubbling fluidization model using kinetic theory of granular flow. *AIChE Journal*, 36(4), 523–538. https://doi.org/10.1002/aic.690360404

Dong, L., Zhang, B., Zhang, Y., Zhao, Y., Zhou, E., Lv, P., & Duan, C. (2017). Kinetic characteristics of the particles in a dense-phase pulsed fluidized bed for dry beneficiation. *Canadian Journal of Chemical Engineering*, *95*(6), 1133–1140. https://doi.org/10.1002/cjce.22751

Dong, L., Zhang, Y., Zhao, Y., Peng, L., Zhou, E., Cai, L., Zhang, B., & Duan, C. (2016). Effect of active pulsing air flow on gas-vibro fluidized bed for fine coal separation. *Advanced Powder Technology*, *27*(5), 2257–2264. https://doi.org/10.1016/j.apt.2016.08.012

Dong, L., Zhu, F., Li, Y., Zhao, Y., Duan, C., Ren, Y., Wang, G., He, J., & Zhang, Y. (2021). Experimental and numerical study of the characteristics of the forced oscillation in a pulsation fluidized bed (PFB) for coal separation. *Chemical Engineering Science*, *234*, 116459. https://doi.org/10.1016/j.ces.2021.116459

Feng, Z., Liu, D., Zhang, W., Feng, H., & Ommen, J. R. Van. (2022). Elutriation and agglomerate size distribution in a silica nanoparticle vibro-fluidized bed. *Chemical Engineering Journal*, *434*(December 2021), 134654. https://doi.org/10.1016/j.cej.2022.134654

Gao, X., Yu, J., Li, C., Panday, R., Xu, Y., Li, T., Ashfaq, H., Hughes, B., Rogers, W. A., Virginia, W., & Virginia, W. (2020). Comprehensive experimental investigation on biomass-glass beads binary

fluidization: A data set for CFD model validation. *AIChE Journal*, *66(2)* 1–18. https://doi.org/10.1002/aic.16843

Ghadirian, E., & Arastoopour, H. (2016). CFD simulation of a fluidized bed using the EMMS approach for the gas-solid drag force. *Powder Technology*, *288*, 35–44. https://doi.org/10.1016/j.powtec.2015.10.034

Gidaspow, D., Bezburuah, R., & Ding, J. (1992). *Hydrodynamics of circulating fluidized beds: Kinetic theory approach*. 7th Fluidization Conference, 75–82. http://www.osti.gov/scitech/servlets/purl/5896246

Huang, D. S., & Levy, E. K. (2004). Heat transfer to fine powders in a bubbling fluidized bed with sound assistance. *AIChE Journal*, *50*(2), 302–310. https://doi.org/10.1002/aic.10028

Ireland, E., Pitt, K., & Smith, R. (2016). A review of pulsed flow fluidisation; the effects of intermittent gas flow on fluidised gas-solid bed behaviour. *Powder Technology*, *292*,108 -121. https://doi.org/10.1016/j.powtec.2016.01.018

Jia, D., Bi, X., Lim, C. J., Sokhansanj, S., & Tsutsumi, A. (2019). Heat transfer in a tapered fluidized bed of biomass particles with pulsed gas flow. *Particuology*, *42*, 2–14. https://doi.org/10.1016/j.partic.2018.01.007

Jia, D., Cathary, O., Peng, J., Bi, X., Lim, C. J., Sokhansanj, S., Liu, Y., Wang, R., & Tsutsumi, A. (2015). Fluidization and drying of biomass particles in a vibrating fl uidized bed with pulsed gas flow. *Fuel Processing Technology*, *138*, 471- 482. https://doi.org/10.1016/j.fuproc.2015.06.023

Köksal, M., & Vural, H. (1998). Bubble size control in a two-dimensional fluidized bed using a moving double plate distributor. *Powder Technology*, *95*(3), 205–213. https://doi.org/10.1016/S0032-5910(97)03337-8

Kunii, D., & Levenspiel, O. (1991). Fluidization engineering. Butterworths, London.

Laverman, J. A., Roghair, I., Van Sint Annaland, M., & Kuipers, H. (2008). Investigation into the hydrodynamics of gas-solid fluidized beds using particle image velocimetry coupled with digital image analysis. *Canadian Journal of Chemical Engineering*, *86*(3), 523–535. https://doi.org/10.1002/cjce.20054

Li, Y., Zhu, F., Zhang, Y., Zhao, Y., Zhang, G., Huang, Q., & Dong, L. (2020a). Characterization of bubble behaviors in a dense phase pulsed gas–solid fluidized bed for dry coal processing. *Particuology*, *1–9*. https://doi.org/10.1016/j.partic.2020.01.002

Li, H. W., Wang, L., Wang, T., & Du, C. he. (2020b). Experimental and CFD-DEM numerical evaluation of flow and heat transfer characteristics in mixed pulsed fluidized beds. *Advanced Powder Technology*, *31*(8), 3144–3157. https://doi.org/10.1016/j.apt.2020.06.004

Li, Y., Zhou, C., Lv, G., Ren, Y., & Zhao, Y. (2021). Prediction of minimum fluidization velocity in pulsed gas – solid fluidized bed. *Chemical Engineering Journal*, *417*(August 2020), 127965. https://doi.org/10.1016/j.cej.2020.127965

Li, Z., Su, W., Wu, Z., Wang, R., & Mujumdar, A. S. (2010). Investigation of flow behaviors and bubble characteristics of a pulse fluidized bed via CFD modeling. *Drying Technology*, *28*(1), 78–93. https://doi.org/10.1080/07373930903430785

Liu, Y. A., Hamby, R. K., & Colberg, R. D. (1991). Fundamental and practical developments of magnetofluidized beds: a review. *Powder Technology*, *64*, 3-41. https://doi.org/10.1016/0032-5910(91)80003-2

Liu, Y., Ohara, H., & Tsutsumi, A. (2016). Pulsation-assisted fl uidized bed for the fl uidization of easily agglomerated particles with wide size distributions. *Powder Technology*, 1–12. https://doi.org/10.1016/j.powtec.2016.12.049

Lun, C. K. K., Savage, S. B., Jeffrey, D. J., & Chepurniy, N. (1984). Kinetic theories for granular flow: Inelastic particles in Couette flow and slightly inelastic particles in a general flow field. *Journal of Fluid Mechanics*, *140*, 223–256. https://doi.org/10.1017/S0022112084000586.

Massimilla, L. (1966). A study on pulsing gas fluidization of beds of particles. *Chemical Engineering Progress*, 62, 63-70.

Mostafaei, F., Golshan, S., Zarghami, R., Gharebagh, R. S., & Mostoufi, N. (2020). Investigating the bubble dynamics in fluidized bed by CFD-DEM. *Powder Technology*, *366*, 938–948. https://doi.org/10.1016/j.powtec.2020.03.011

Namdarkedenji, R., Hashemnia, K., & Emdad, H. (2018). Effect of flow pulsation on fluidization degree of gas-solid fluidized beds by using coupled CFD-DEM. *Advanced Powder Technology*, *29*(12), 3527–3541. https://doi.org/10.1016/j.apt.2018.09.033

Nitz, M. (2007). Drying of beans in a pulsed fluid bed dryer: Drying kinetics, fluid-dynamic study and comparisons with conventional fluidization. *Journal of Food Engineering*, 80, 249–256. https://doi.org/10.1016/j.jfoodeng.2006.05.025

Ogawa, S., Umemura, A., Oshima, N., & Physics, I. (1980). On the equations of fully fluidized granular materials. *Journal of Applied Mathematics and Physics*, *31*, 483-493. https://doi.org/10.1007/BF01590859

Reuge, N., Cadoret, L., Coufort-saudejaud, C., Pannala, S., Syamlal, M., & Caussat, B. (2008). Multifluid Eulerian modeling of dense gas – solids fluidized bed hydrodynamics: Influence of the dissipation parameters. *Chemical Engineering Science*, *63*, 5540–5551. https://doi.org/10.1016/j.ces.2008.07.028

Sau, D. C., Mohanty, S., & Biswal, K. C. (2010). Experimental studies and empirical models for the prediction of bed expansion in gas-solid tapered fluidized beds. *Chemical Engineering and Processing: Process Intensification*, *49*(4), 418-424. https://doi.org/10.1016/j.cep.2010.02.010

Schaeffer, D. G. (1987). Instability in the evolution equations describing incompressible granular flow. *Journal of Differential Equations*, *66*(1), 19–50. https://doi.org/10.1016/0022-0396(87)90038-6

Shah, M. T., Utikar, R. P., & Pareek, V. K. (2016). CFD study: Effect of pulsating flow on gas–solid hydrodynamics in FCC riser. *Particuology*, *31*, 25-34. https://doi.org/10.1016/j.partic.2016.07.002

Syamial, M., & O'Brien, T. J. (1989). *Computer simulation of bubbles in a fluidized bed.* Fluidization and Fluid Particle Systems: Fundamentals and Applications. New York, U.S.A., American Institute Chemical Engineers.

Syamlal, M., Rogers, W., & O`Brien, T. J. (1993). *MFIX documentation theory guide.* U.S. Department of Energy Office of Fossil Energy. https://doi.org/10.2172/10145548

Taghipour, F., Ellis, N., & Wong, C. (2005). Experimental and computational study of gas-solid fluidized bed hydrodynamics. *Chemical Engineering Science*, *60*, 6857-6867. https://doi.org/10.1016/j.ces.2005.05.044

Van Willigen, F. K., Van Ommen, J. R., Van Turnhout, J., & Van den Bleek, C. M. (2005). Bubble size reduction in electric-field-enhanced fluidized beds. *Journal of Electrostatics*, *63*(6-10), 943-948. https://doi.org/10.1016/j.elstat.2005.03.065

Wachem, B. G. M. Van, Schouterf, J. C., Krishnab, R., & Bleek, C. M. Van Den. (1998). Eulerian simulations of bubbling behaviour in gas-solid fluidised beds. *Computers & Chemical Engineering*, *22*, 299-306.

Wang, X. S., & Rhodes, M. J. (2005). Pulsed fluidization - A DEM study of a fascinating phenomenon. *Powder Technology*, *159*(3), 142–149. https://doi.org/10.1016/j.powtec.2005.08.007

Wong, H. W., & Baird, M. H. I. (1971). Fluidisation in a pulsed gas flow. *The Chemical Engineering Journal*, *2*(2), 104–113. https://doi.org/10.1016/0300-9467(71)80004-7

Zhang, D., & Koksal, M. (2006). Heat transfer in a pulsed bubbling fluidized bed. *Powder Technology*, *168*, 21–31. https://doi.org/10.1016/j.powtec.2006.06.017

Zhu, C., Liu, G., Yu, Q., Pfeffer, R., Dave, R. N., & Nam, C. H. (2004). Sound assisted fluidization of nanoparticle agglomerates. *Powder Technology*, 141, 119–123. https://doi.org/10.1016/j.powtec.2004.01.023